Kidney Diseases

Research Article

Kidney Dis
DOI: 10.1159/000529995

Received: November 28, 2022
Accepted: February 16, 2023
Published online: March 17, 2023

Nephropathy Is Aggravated by Fatty Acids in Diabetic Kidney Disease through Tubular Epithelial Cell Necroptosis and Is Alleviated by an RIPK-1 Inhibitor

Qi Yu[a, b, c] Ying Chen[a, b, c, d, e] Youlu Zhao[a, b, c, d, e] Shuo Huang[a, b, c] Xiaohong Xin[a, b, c] Lei Jiang[a, b, c, d, e] Hui Wang[f] Wenyan Wu[a, b, c] Lei Qu[a, b, c] Chengang Xiang[a, b, c, d, e] Suxia Wang[f] Gang Liu[a, b, c, d, e] Li Yang[a, b, c, d, e]

[a]Renal Division, Renal Pathology Center, Peking University First Hospital, Beijing, China; [b]Institute of Nephrology, Peking University, Beijing, China; [c]Key Laboratory of Renal Disease, Ministry of Health of China, Beijing, China; [d]Key Laboratory of CKD Prevention and Treatment (Peking University), Ministry of Education of China, Beijing, China; [e]Research Units of Diagnosis and Treatment of Immune-mediated Kidney Diseases, Chinese Academy of Medical Sciences, Beijing, China; [f]Laboratory of Electron Microscopy, Pathological Center, Peking University First Hospital, Beijing, China

Keywords
Diabetic kidney disease · Necroptosis · Phosphorylated MLKL · Fatty acids · Renal tubular epithelial cells

Abstract
Introduction: Diabetic kidney disease (DKD), one of the leading causes of end-stage renal disease, has complex pathogenic mechanisms and few effective clinical therapies. DKD progression is accompanied by the loss of renal resident cells, followed by chronic inflammation and extracellular matrix deposition. Necroptosis is a newly discovered form of regulated cell death and is a major form of intrinsic cell loss in certain diabetic complications such as cardiomyopathy, intestinal disease, and retinal neuropathy; however, its significance in DKD is largely unknown. ***Methods:*** In this study, the expression of necroptosis marker phosphorylated MLKL (p-MLKL) in renal biopsy tissues of patients with DKD was detected using immunofluorescence and semiquantified using immunohistochemistry. The effects of different disease-causing factors on necroptosis activation in human HK-2 cells were evaluated using immunofluorescence and Western blotting. *db/db* diabetic mice were fed a high-fat diet to establish an animal model of DKD with significant renal tubule damage. Mice were treated with the RIPK1 inhibitor RIPA-56 to evaluate its renal protective effects. mRNA transcriptome sequencing was used to explore the changes in signaling pathways after RIPA-56 treatment. Oil red O staining and electron macroscopy were used to observe lipid droplet accumulation in renal biopsy tissues and mouse kidney tissues. ***Results:*** Immunostaining of phosphorylated RIPK1/RIPK3/MLKL verified the occurrence of necroptosis in renal tubular epithelial

Qi Yu and Ying Chen contributed equally to this work.

karger@karger.com
www.karger.com/kdd

Correspondence to:
Ying Chen, ychen0822@126.com
Li Yang, li.yang@bjmu.edu.cn

cells of patients with DKD. The level of the necroptosis marker p-MLKL correlated positively with the severity of renal functional, pathological damages, and lipid droplet accumulation in patients with DKD. High glucose and fatty acids were the main factors causing necroptosis in human renal tubular HK-2 cells. Renal function deterioration and renal pathological injury were accelerated, and the necroptosis pathway was activated in *db/db* mice fed a high-fat diet. Application of RIPA-56 effectively reduced the degree of renal injury, inhibited the necroptosis pathway activation, and reduced necroinflammation and lipid droplet accumulation in the renal tissues of *db/db* mice fed a high-fat diet. ***Conclusion:*** The present study revealed the role of necroptosis in the progression of DKD and might provide a new therapeutic target for the treatment of DKD.

Introduction

The global prevalence of diabetes mellitus, especially type 2 diabetes mellitus secondary to obesity and metabolic syndromes, has increased dramatically in recent decades [1]. Kidneys are one of the most commonly affected organs in diabetes mellitus; approximately 30~40% of diabetic patients will progress to diabetic kidney disease (DKD) [1]. DKD has become the leading cause of chronic kidney disease, eventually progressing to end-stage renal disease in some patients [2]. During DKD progression, persistent metabolic disorders can cause imbalances in cell signaling pathways and induce cytotoxic cytokine production, ultimately leading to renal cell death [3].

Necroptosis is a newly discovered type of regulated cell death that has similar morphological features (cell swelling, rupture, and chromatin condensation) to those of cell apoptosis but involves different molecular pathways [4, 5]. It is triggered by death receptors such as tumor necrosis factor receptor 1 (TNFR1) or the FAS receptor. Its mechanism of action involves inhibition of caspase-8 activity and the formation of complexes I and II and necrosomes by RIPK1-RIPK3-MLKL. Finally, MLKL is phosphorylated and anchored in the cell membrane, leading to membrane rupture and leakage of intracellular contents and causing inflammatory responses [6–8].

In human kidney biopsy specimens, TdT-mediated dUTP-biotin nick end-labeling (TUNEL)-positive signals were detected in podocytes, renal tubular epithelial cells (RTECs), and interstitial cells [9–11], indicating the cell death of renal resident cells. Necroptosis is an important inflammatory cell death pathway that drives the pathology of multiple degenerative diseases, including Alzheimer's disease and type 2 diabetes mellitus [12–16]. However, reports on the role of necroptosis in DKD are limited. Therefore, we investigated the relationship between necroptosis and DKD in human patients, explored the causal factors of necroptosis activation in human renal epithelial cells, and evaluated the therapeutic potential of the RIPK1 inhibitor RIPA-56 to treat diabetic-related nephropathy in high-fat diet-fed *db/db* mice.

Materials and Methods

Clinical Samples

Patients with DKD were enrolled according to clinical and pathological criteria at Peking University First Hospital from January 2012 to December 2016. Patients who were diagnosed with DKD with primary and secondary glomerular disease or DKD with thrombotic microangiopathies and small vasculitis were excluded. Thirty human DKD kidney tissues were obtained from renal biopsy, and ten para-carcinoma normal kidney tissues from age- and sex-matched patients were obtained as controls.

Renal Pathology of Patients with DKD

Formalin-fixed and paraffin-embedded (FFPE) human kidney sections (2.5 μm) were stained with hematoxylin and eosin (H&E), periodic acid-Schiff (PAS), Masson's trichrome, and periodic-acid-silver methermaine plus Masson's trichrome (PASM+Masson) solutions for light microscopy evaluation. Kidney histopathological lesions were evaluated in all components of the renal cortex, including the glomeruli, arterioles, and tubulointerstitium, as described previously [17]. Blinded semiquantitative scoring of the percentage of the parenchyma affected by the lesions was performed by two experienced renal pathologists. Ten to 15 randomly selected nonoverlapping fields were scored for each patient. The detailed scales for scoring the pathological lesions can be found in online supplementary Table S1 (for all online suppl. material, see www.karger.com/doi/10.1159/000529995). The clinical and pathological parameters of the 30 DKD patients are summarized in online supplementary Table S2.

Cell Culture

Human renal tubular epithelial cells (HK-2) were purchased from Procell Life Science & Technology Company (CL-0109, Wuhan, China). HK-2 cells were cultured in minimum essential medium with 10% fetal bovine serum and 1% penicillin/streptomycin at 37°C in a 5% CO_2 humidified incubator. After synchronization by serum-free minimum essential medium for 12 h, HK-2 cells were stimulated with high glucose (HG, 30 mmol/L), palmitic acid (PA, 300 μmol/L), high glucose plus palmitic acid (HGPA, HG 30 mmol/L plus PA 300 μmol/L), advanced glycation end products (100 μg/mL), and BSA (10 mg/mL). Necrostatin-1 (Nec-1, 10 μM, N9037, Sigma Aldrich) or RIPA-56 (100 nM, Sironax, Beijing, China) were used to pretreat HK-2 cells for 1 h, and then Nec-1 or RIPA-56 plus HGPA was used to stimulate HK-2 cells for 24 h.

Animal Experiments

C57BLKS-Lepr^{db} (*db/db*) mice (strain no. T002407) and C57BLKS-Lepr^{wt} (*wt/wt*) mice (8 weeks old, all males) were purchased from GemPharmatech Co., Ltd. (license number: SCXK (Su) 2018-0008, Nanjing, China). The baseline levels of fasting blood glucose, body weight, blood urea nitrogen (BUN), and albumin-to-creatinine ratio (ACR) of mice on a regular diet were measured routinely. High-fat mouse chow with 60 kcal% (D1292) was purchased from Xietong Biotechnology Company (Nanjing, China). For the high-fat-diet mouse model, 14-week-old mice were randomly divided into four groups: *wt/wt* mice fed a regular diet (wt-RD), *wt/wt* mice fed a high-fat diet (wt-HFD), *db/db* mice fed a regular diet (db-RD), and *db/db* mice fed a high-fat diet (db-HFD), and observed for 2 weeks.

RIPA-56 Feeding Experiment

RIPA-56 was mixed into mouse chow at a dose of 300 mg/kg as previously described [18] and pre-fed to 13-week-old *db/db* mice and *wt/wt* mice for 1 week. Then, the mice were randomly divided into four groups: *wt/wt* mice fed a high-fat diet (wt-HFD), *wt/wt* mice fed a high-fat diet plus RIPA-56 (wt-HFD+R), *db/db* mice fed a high-fat diet (db-HFD), and *db/db* mice fed a high-fat diet plus RIPA-56 (db-HFD+R), and they were maintained on each diet for 36 days. Body weight, fasting blood glucose, BUN, and ACR were measured weekly. At the end of each experiment, the animals were euthanized using an overdose of pentobarbital sodium. The hearts were perfused with 10 mL of ice-cold PBS before the kidneys were collected for subsequent experiments.

Assessment of Renal Function

Mouse serum urea nitrogen was detected using the Urea Assay Kit (DIUR-500, Bioassay System, Hayward, CA, USA), urinary albumin was detected using the Mouse Albumin Elisa Kit (A90-134A, Bethyl Laboratories, Montgomery, TX, USA), and urinary creatinine was detected using the QuantiChrom™ Creatinine Assay Kit (DICT-500, Bioassay System, Hayward, CA, USA). The urinary ACR was calculated as urinary albumin divided by urinary creatinine.

Renal Pathology of the db/db Mice

FFPE mouse kidney sections were stained with PAS solution. To evaluate mesangial matrix hyperplasia, images of ten glomeruli from each kidney section were taken under ×400 magnification. The mesangial matrix area was defined as the PAS-positive and nucleus-free region and was measured using Image Pro Plus (Media Cybernetics, Rockville, MD, USA). The mesangial matrix expansion index was defined as the mesangial matrix area divided by the total glomerular area. Glomerular size was calculated as the average of the long and short glomerular diameters. Tubular vacuolar degeneration scoring was based on a 0 to 4 scale (0, no lesions, $0 < 0.5 \leq 10\%$, $10\% < 1 \leq 25\%$, $25\% < 2 \leq 50\%$, $50\% < 3 \leq 75\%$, $75\% < 4 \leq 100\%$) and observed by light microscopy (Leica DM2500, Weltzlar, Germany) at a high-power field. Ten to 15 randomly selected nonoverlapping fields were scored for each mouse, and the averages for each group were compared.

Immunofluorescence and Immunohistochemistry of Kidney Tissues

FFPE kidney tissue sections were deparaffinized in xylene and rehydrated in gradient ethanol. Antigen retrieval was performed by boiling the specimens in sodium citrate buffer (pH 6.0) with 0.5% Tween-20 for 3 min and then blocking them with 3% BSA at room temperature for 1 h. The specimens were incubated with phosphorylated MLKL (p-MLKL) primary antibody (ab187091, Abcam, Cambridge, UK) at 4°C overnight, and then incubated with HRP-conjugated secondary antibody (PV6001, ORIGENE, Beijing, China), detected with diaminobenzene (DAB) solution, and counterstained with hematoxylin to label the nuclei. Digital images of p-MLKL staining in the tubulointerstitium were acquired using a DM2500 light microscope (Leica, Germany) under ×400 magnification. Image Pro Plus 6.0 software was used to measure the integrated optical density (IOD) of each image, and the mean IOD value of ten images was calculated for each patient.

For immunofluorescence, after rehydration, antigen retrieval, and blockade of nonspecific binding, FFPE sections were incubated with primary antibodies recognizing RIPK3 (10188, CST, Danvers, MA, USA), p-RIPK3 (ab195117, Abcam, Cambridge, UK), MLKL (ab184718, Abcam), and p-MLKL overnight at 4°C and then incubated with Cy3-labeled goat anti-rabbit IgG (A0516, Beyotime, Shanghai, China), and the nuclei were counterstained using 4′,6-diamidino-2-phenylindole (DAPI, ZLI-9557, ORIGENE). Staining was examined under a Zeiss LSM 780 confocal microscope (Carl Zeiss, Berlin, Germany).

Immunocytochemistry and TUNEL Staining

After culturing on coverslips and stimulation for 24 h, HK-2 cells were fixed with 4% paraformaldehyde and permeabilized with 0.3% Triton X-100. After blocking with 3% BSA, the cells on coverslips were incubated with anti-p-MLKL antibody (ab187091, Abcam), followed by incubation with Cy3-labeled goat anti-rabbit secondary antibody, counterstained with DAPI, and observed under a Zeiss LSM 780 confocal microscope. For the TUNEL assay, HK-2 cells were fixed and permeabilized as described above. A mixture of fluorescein-dUTP and TdT enzyme solution was incubated with the cells at 37°C for 1 h. All the coverslips were counterstained with DAPI and observed under a Zeiss LSM 780 confocal microscope.

Transmission Electron Microscopy

Kidney tissues were fixed, dehydrated, and embedded as described previously [19]. After staining with 2% uranyl acetate and lead citrate, ultra-thin sections (50 nm) were acquired and examined using a transmission electron microscope (JEM-1230; JEOL Ltd., Tokyo, Japan) under 6,000 × magnification.

Oil Red O Staining

Frozen kidney sections (6 μm) were soaked in 60% isopropanol for 20–30 s, then stained with modified oil red O staining solution (G1261, Solarbio, Beijing, China) for 15 min, followed by counterstaining of the nuclei using Mayer's hematoxylin.

Western Blotting

Total proteins from mouse kidneys or HK-2 cells were extracted using RIPA buffer (P0013B, Beyotime, Shanghai, China) supplemented with protease inhibitors (4693116001, Roche, Basel, Switzerland) and phosphatase inhibitors (4906845001, Roche). The denatured proteins were separated by

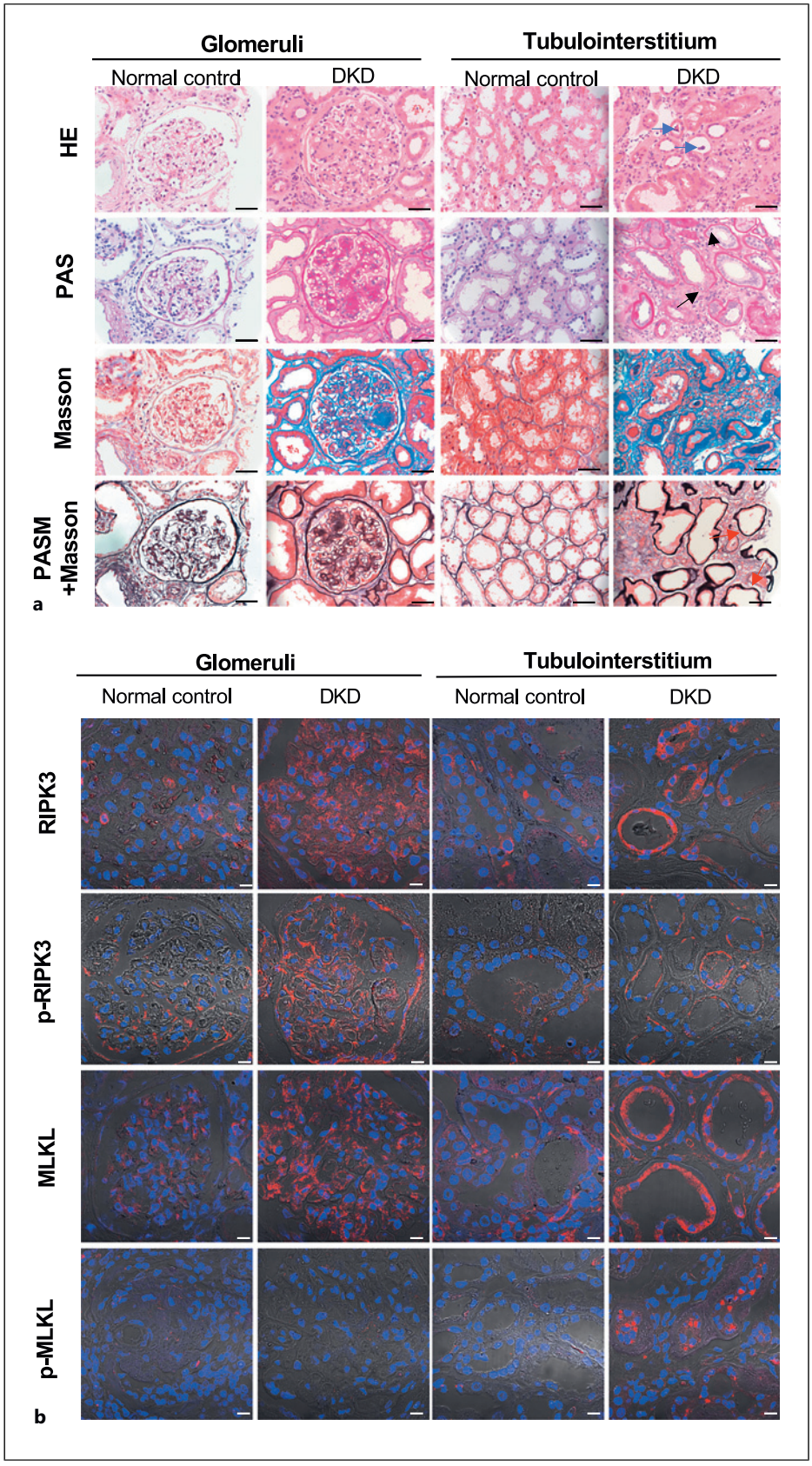

Fig. 1. Detection of necroptosis in kidney specimens from patients with DKD. **a** Staining of kidney specimens including hematoxylin-eosin staining (H&E), periodic acid-Schiff staining (PAS), Masson's trichrome staining (Masson), and periodic acid-silver methenamine plus Masson's trichrome staining (PASM+-Masson). Blue arrows indicate sloughing of the tubular epithelial cells; short black arrows indicate karyopyknosis; long black arrows indicate karyorrhexis; red arrows indicate nearly naked tubular basement membrane. Scale bar, 50 μm. **b** Immunofluorescence staining of RIPK3, p-RIPK3, MLKL, p-MLKL in kidney specimens. Scale bar, 10 μm.

a 4–12% gradient gel and then transferred onto a PVDF membrane, blocked with 5% nonfat dry milk, and incubated with primary antibodies overnight at 4°C. The primary antibodies included: anti-mouse/human RIPK1 (3493, CST), anti-human p-RIPK1 (65746, CST), anti-mouse p-RIPK1 (38662, CST), anti-human MLKL (ab184718, Abcam), anti-mouse MLKL (37705, CST), anti-human p-MLKL (ab187091, Abcam), anti-mouse p-MLKL (ab196436, Abcam), anti-human/mouse caspase-3 (9662, CST), anti-human/mouse cleaved caspase-3 (9661, CST), anti-mouse NGAL (sc-515876, Santa Cruz). The membranes were incubated with HRP-conjugated secondary antibodies, then developed with Immobilon ECL Ultra Western HRP substrate (WBULS0500, Millipore, USA). Images were captured with an ImageQuant LAS 4000 Microsystem (GE, Healthcare). The relative intensities of each protein band were quantified using ImageJ software. β-actin levels were used as internal controls.

RNA Sequencing

RNA was extracted from mouse kidney tissues and subjected to first-strand cDNA synthesis for library preparation. Thirty million paired-end, 100 bp reads for each sample were generated using a NovaSeq 6000 sequencer (Illumina, San Diego, CA, USA). The sequences were aligned to the murine genome (10 mm) by STAR (2.7.5c), and StringTie (v2.1.7) was used to obtain the standardized fragments per kilobase of exon model per million mapped fragments (FPKM) value. DEseq2* (Bioconductor, Boston, MA, USA) was used to analyze the difference in the gene count matrix. edgeR* (Bioconductor) was used to perform difference analysis on the grouping of non-duplicate samples. Significantly upregulated and downregulated genes ($p < 0.01$) were analyzed separately for enrichment of Kyoto Encyclopedia of Genes and Genomes (KEGG) pathways using the DAVID bioinformatics platform with a false discovery rate threshold of <0.05 [20].

Quantitative Real-Time Reverse Transcription PCR

A total RNA extraction kit (DP419, Tiangen, Beijing, China) was used to extract total RNA from mouse kidney tissues according to the manufacturer's operating procedures. 1 μg of total RNA was reverse transcribed into cDNA (R333-01, Vazyme, Nanjing, China). SYBR Green Mix (A25742; Applied Biosystems, Foster City, CA, USA) was used to prepare real-time PCR reagents, and PCRs were performed on an ABI Vii7 System. The primers used are listed in online supplementary Table S3.

Statistical Analysis

GraphPad Prism 8.0 (GraphPad Software, Inc., La Jolla, CA, USA) was used for statistical analysis. Normally distributed data are presented as the mean ± standard deviation and were analyzed by *t* test or one-way ANOVA. Non-normally distributed data are presented as the median (maximum, minimum) and analyzed by a rank sum test. Pearson correlation or Spearman correlation was used for correlation analysis. Categorical variables are described by frequency (percentage), using the χ^2 test or Fisher's exact test. All *p* values are two-tailed, and differences were considered statistically significant at $p < 0.05$.

Results

Necroptosis Occurred in Renal Tubular Epithelial Cells from Patients with DKD

Thirty patients, 21 males and 9 females, aged 43.13 ± 12.83 years, who were clinically and pathologically diagnosed with DKD at Peking University First Hospital from January 2012 to December 2016 were enrolled (online suppl. Table S1). Their mean serum creatinine level at peak was 249.68 ± 184.42 μmol/L, and their mean estimated glomerular filtration rate was 43.13 ± 30.33 mL/min/1.73 m^2. Light microscopy evaluation of renal biopsy specimens from patients with DKD showed a diffuse increase in the mesangial matrix and some Kimmelstiel-Wilson nodules in individual glomeruli and marked periglomerular and tubulointerstitial fibrosis. Lesions such as vacuolar degeneration, flattening and sloughing of tubular epithelial cells, scattered cell death manifested as karyopyknosis and karyorrhexis, and nearly naked tubular basement membranes were also observed (Fig. 1a). The control specimens appeared normal (Fig. 1a).

Routine pathological tests usually fail to distinguish necroptotic cells from apoptotic cells. To determine the underlying cause of renal cell death, representative molecules in necroptotic pathways in kidney tissues from patients with DKD were evaluated. Positive staining of RIPK3, p-RIPK3, and MLKL was observed in glomeruli and tubules. However, the necroptosis executor p-MLKL was mainly stained in renal tubules. These results confirmed that renal tubular cells underwent necroptosis during DKD (Fig. 1b).

Correlation of p-MLKL Expression with the Severity of Renal Functional and Pathological Damage in Patients with DKD

IHC staining of p-MLKL in kidney tissues was performed, and the IOD of p-MLKL in the tubulointerstitium was used for semi-quantitative analysis (Fig. 2a). The 30 patients were classified into class II (16 cases) and class III (14 cases) DKD according to the Tervaert pathological classification criteria for diabetic nephropathy [21]. Positive expression of p-MLKL was found in 73.3% (22/30, $p < 0.001$) of all patients with DKD, in 62.5% (10/16, $p = 0.0532$) of patients with class II DKD, and in 85.7% (12/14, $p < 0.001$) of patients with class III DKD (Fig. 2b). In the tubulointerstitium, p-MLKL levels in class III DKD patients were significantly higher than those in class II DKD patients (Fig. 2c).

Correlation analysis between tubulointerstitial levels of p-MLKL and the clinicopathological parameters of

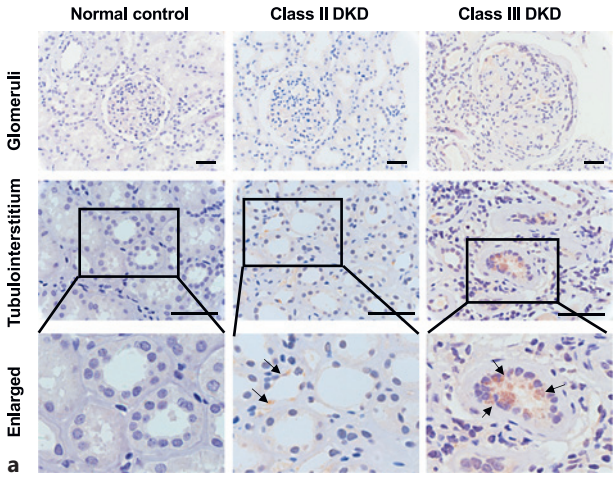

Group	Normal (n=10)	DKD			p value
		Total (n=30)	Class II (n=16)	Class III (n=14)	
p-MLKL positive n (%)	0 (0)	22 (73.3)[a]	10 (62.5)[b]	12 (85.7)[c]	<0.001

a Total DKD vs normal, $p<0.001$, Chi-square test;
b Class II DKD vs normal, $p=0.0532$; c Class III DKD vs normal, $p<0.001$, Fisher's exact test.

b

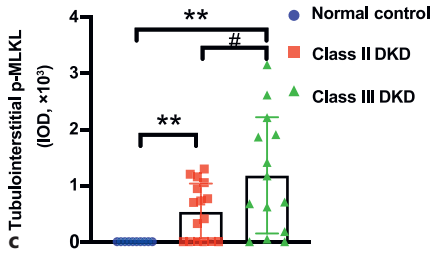

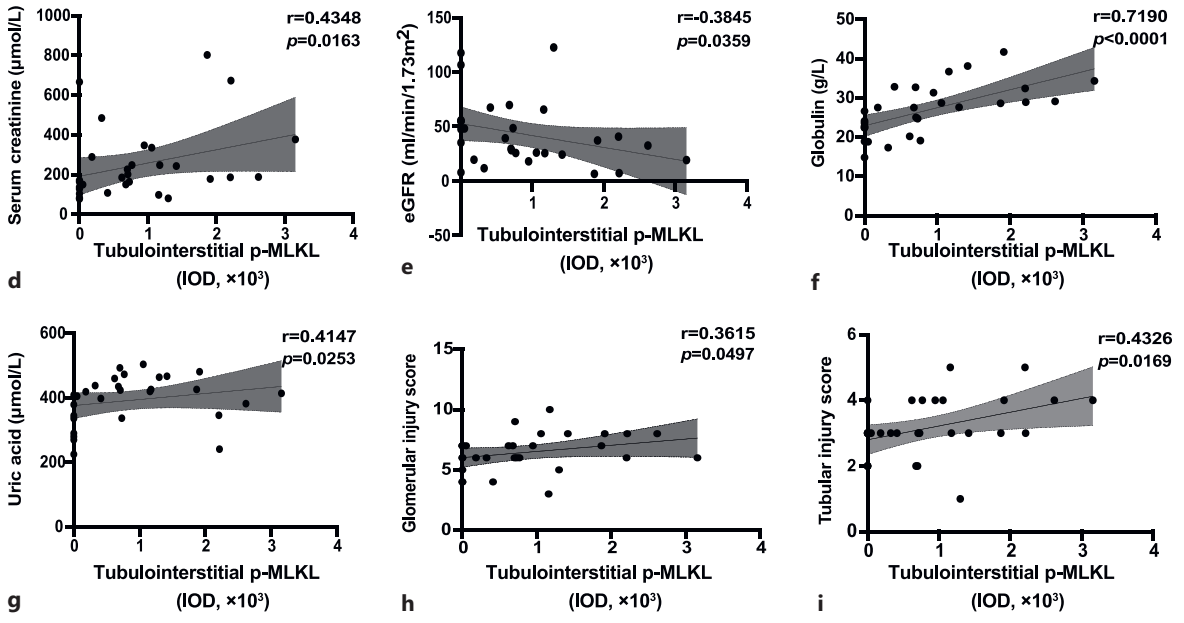

Fig. 2. Tubulointerstitial p-MLKL levels correlated with the severity of renal damage in DKD patients. **a** Immunohistochemistry staining of p-MLKL in kidney specimens of DKD patients. Black arrows indicate p-MLKL positive signals. Scale bar, 50 μm. **b** Percentage of *p*-MLKL positive expression in DKD patients. **c** Comparison of tubulointerstitial p-MLKL levels in class II and class III DKD patients. $^{**}p < 0.01$ compared to normal control, $^{\#}p < 0.05$ compared to Class II DKD. **d**–**i** Correlation of tubulointerstitial p-MLKL levels with serum creatinine (**d**), eGFR (**e**), globulin (**f**), uric acid (**g**), glomerular injury score (**h**), and tubular injury score (**i**). eGFR, estimated glomerular filtration rate.

the patients with DKD showed that p-MLKL IOD correlated positively with peak serum creatinine (r = 0.4348, p = 0.0163), globulin (r = 0.7190, $p < 0.0001$), and uric acid (r = 0.4147, p = 0.0253) but correlated negatively with estimated glomerular filtration rate (r = −0.3845, p = 0.0359). Correlation analysis showed that the *p*-MLKL IOD had a stronger association with the tubular injury score (r = 0.4326, p = 0.0169) than with the glomerular injury score (r = 0.3615, p = 0.0497) (Fig. 2d–i).

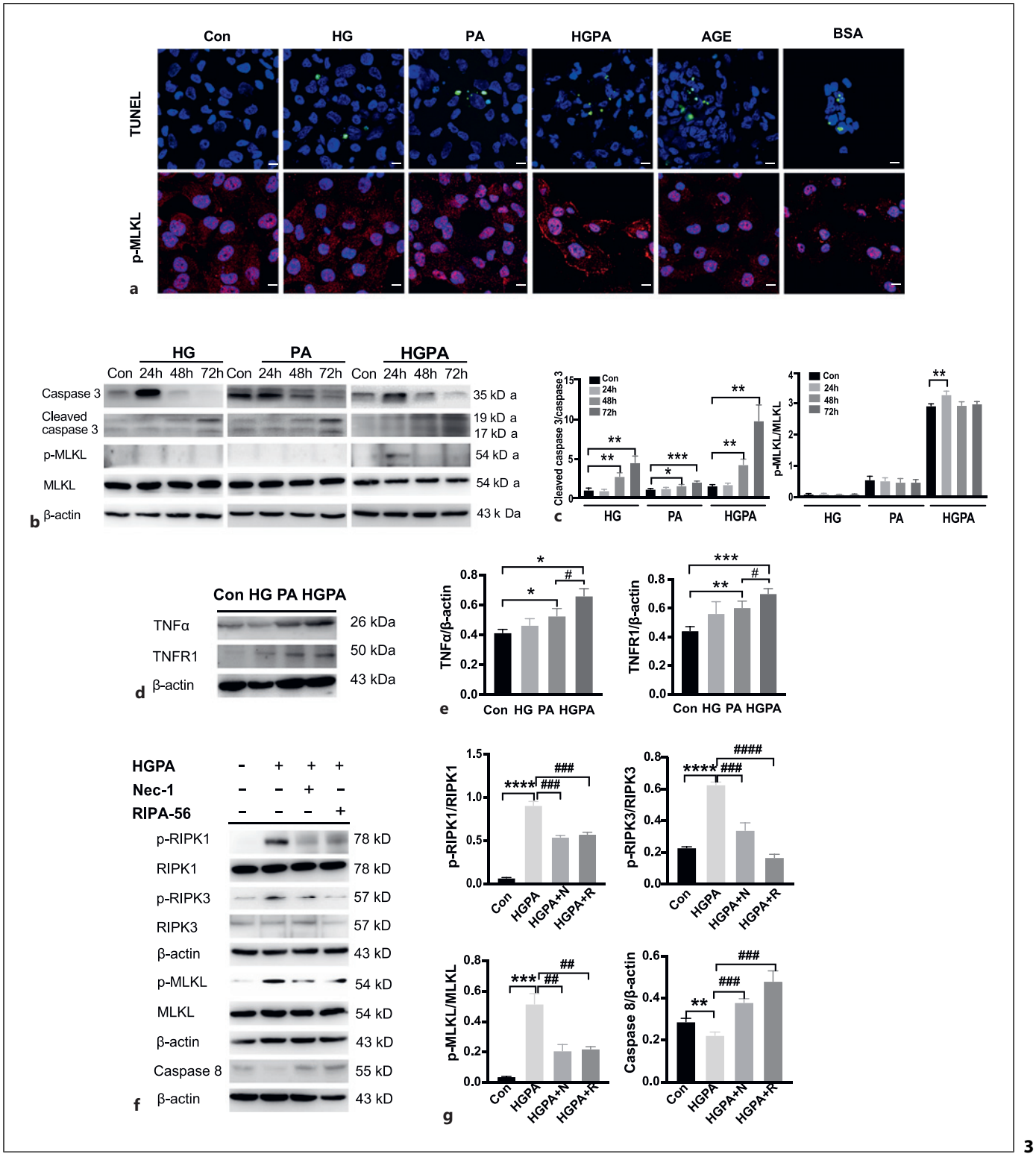

3

(For legend see next page.)

High Glucose and Fatty Acids Were the Main Factors Causing Necroptosis in Renal Tubular Cells

To explore which factors activate necroptosis in RTECs, we administered HG, PA, HGPA, advanced glycation end products, and BSA to HK-2 cells for 24 h to observe necroptotic pathway activation. All five treatments induced TUNEL-positive signals (Fig. 3a); however, necroptosis-specific membrane translocation of p-MLKL was detected only under HGPA stimulation, indicating that high glucose combined with fatty acids could be the main activators of necroptosis in RTECs (Fig. 3a).

To further confirm the necroptotic mechanisms in RTECs in response to HGPA, we first compared the activation of apoptosis and necroptosis pathways in HK-2 cells after prolonged stimulation by HG, PA, and HGPA for 72 h. The expression of the apoptosis marker cleaved caspase-3 increased gradually with a concomitant decrease in total caspase-3 after 72 h of stimulation; however, the levels of the necroptosis marker p-MLKL increased only after HGPA stimulation (Fig. 3b–c). TNFα directly induces cell necroptosis. Therefore, TNFα levels were detected in HK-2 cells stimulated with HG, PA, and HGPA for 24 h. HG hardly induced TNFα expression, whereas PA stimulation increased TNFα expression compared with that in the control. HGPA further increased the expression of TNFα (Fig. 3d–e). TNFR1 expression also increased under HGPA stimulation (Fig. 3d–e). Next, HGPA-induced HK-2 cells were treated with the necroptosis inhibitor Nec-1 and the novel RIPK-1 inhibitor RIPA-56. HGPA treatment induced increased levels of p-RIPK1/p-RIPK3/p-MLKL and inhibited caspase-8 (Fig. 3f–g). This necroptosis activation was suppressed by Nec-1 (10 μM) or lower dose of RIPA-56 (100 nM).

We further performed oil-red O staining. There was almost no oil red O staining in the normal control kidney tissues (Fig. 4a). In the DKD samples with little oil red O staining, p-MLKL levels were also lower in the renal tubules, whereas in DKD samples with marked oil red O positive lipid droplet deposition, higher p-MLKL levels were observed in the tubulointerstitial region (Fig. 4a). Eight patients with DKD were selected and their samples were subjected to both oil red O staining and p-MLKL immunofluorescence staining. There was a significant positive correlation between the intensity of oil red O staining and p-MLKL levels ($r = 0.8014$, $p = 0.0168$), suggesting the amount of lipid deposition is accompanied by necroptosis activation in the renal tubular epithelium of patients with DKD (Fig. 4b).

Nephropathy Was Aggravated and Necroptosis Was Activated by High-Fat Diet in Diabetic db/db Mice

To verify the clinical and in vitro findings, we used a classic type 2 diabetes mouse model, the C57BLKS-Lepr^{db} (*db/db*) mice, and checked their DKD symptoms. Under an RD, the body weight and blood glucose level of the *db/db* mice were higher than those of the *wt/wt* mice (Fig. 5a). Although BUN and ACR were higher in the *db/db* mice than in the *wt/wt* mice, kidney pathological changes were mainly observed in the glomeruli with mild mesangial matrix hyperplasia; however, there were no obvious pathological changes in the renal tubulointerstitium in the *db/db* mice (Fig. 5b, c).

Since there was only mild nephropathy and no obvious tubule injury in the RD-fed *db/db* mice, the *db/db* mice were fed with an HFD to observe renal damage. The body weight and blood glucose level were greatly increased in *db/db* mice after HFD feeding (Fig. 5d). Renal function also decreased rapidly, which was manifested by increased BUN and ACR after HFD feeding (Fig. 5d). The pathological damage to renal tissue was significantly aggravated in HFD-fed *db/db* mice. The mesangial matrix area was further increased in *db/db* mice fed an HFD for 2 weeks (Fig. 5e, f). In the tubulointerstitial region, swelling of RTECs, brush border shedding, and vacuolar degeneration were observed in HFD-fed *db/db* mice, which was not observed in RD-fed *db/db* mice (Fig. 5e, f).

The levels of the key necroptosis pathway proteins, p-RIPK1, RIPK1, p-MLKL, and MLKL, in mouse kidney

Fig. 3. HGPA stimulated necroptosis in RTECs. **a** TUNEL (green) and p-MLKL (red) staining in different factors-stimulated HK2 cells. Scale bar, 10 μm. **b, c** Caspase-3, cleaved caspase-3, p-MLKL, MLKL levels in HG, PA, or HGPA stimulated HK2 cells for 24 h, 48 h or 72 h treatment. $^{*}p < 0.05$, $^{**}p < 0.01$, $^{***}p < 0.001$ compared to control ($n = 3$). **d, e** TNFα, TNFR1 levels in HG, PA or HGPA stimulated HK2 cells for 24 h treatment. $^{*}p < 0.05$, $^{**}p < 0.01$, $^{***}p < 0.001$ compared to control; $^{\#}p < 0.05$, compared to PA stimulation ($n = 3$). **f, g** HK2 cells were stimulated with HGPA, HGPA plus Nec-1 (10 μm), HGPA plus RIPA-56 (100 nM) and detected for p-RIPK1/RIPK1, p-RIPK3/RIPK3, p-MLKL/MLKL and caspase-8 expression. $^{**}p < 0.01$, $^{***}p < 0.001$, $^{****}p < 0.0001$ compared to control; $^{\#\#}p < 0.01$, $^{\#\#\#}p < 0.001$, $^{\#\#\#\#}p < 0.0001$ compared to HGPA stimulation ($n = 3$). Statistical significance was analyzed by two-sided Student's *t* test. HG: high glucose; PA: palmitic acid; HGPA: high glucose plus palmitic acid; AGE: advanced glycation end products; BSA: bovine serum albumin.

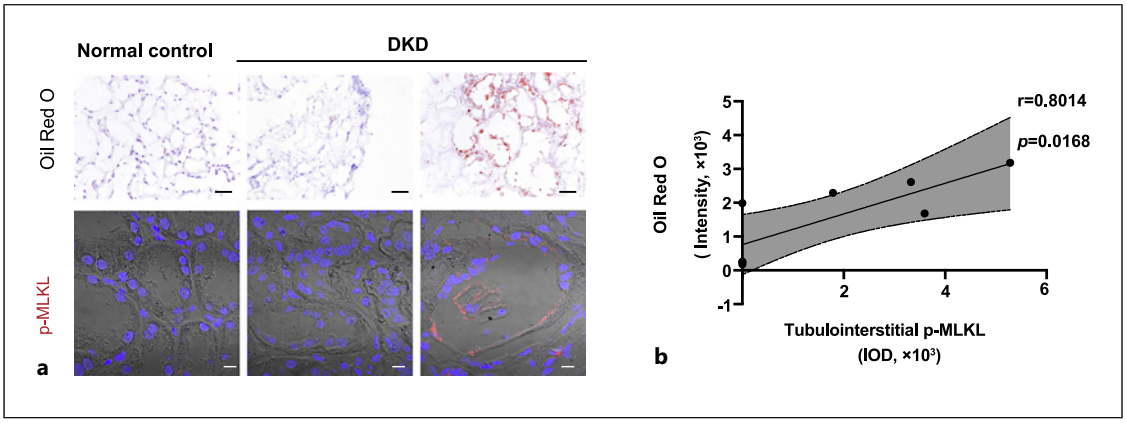

Fig. 4. Correlation between lipid deposition and p-MLKL expression in tubulointerstitium of DKD patients. **a** Representative images of oil red O staining (scale bar, 50 μm) and p-MLKL immunofluorescence staining (scale bar, 10 μm) in Normal control and DKD patients. **b** Correlation analysis of oil red O staining intensity and p-MLKL IOD in tubulointerstitium of DKD patients (n = 8).

tissues were assessed. The changes of necroptosis markers p-RIPK1 and p-MLKL were not detected in the kidney tissues of 22-week-old RD-fed *db/db* mice compared to age-matched *wt/wt* mice (Fig. 5g, h). However, p-RIPK1 or p-MLKL levels were significantly upregulated in the db-HFD group compared to wt-HFD group (Fig. 5i, j) as well as db-RD group (Fig. 5k, l), suggesting that necroptosis was activated by an HFD in the *db/db* mice.

The RIPK-1 Inhibitor RIPA-56 Reduced the Degree of Renal Injury and Inhibited the Necroptosis Pathway in db/db Mice Fed a High-Fat Diet

Next, an animal model was constructed by orally feeding HFD *db/db* mice with RIPA-56 to chronically inhibit the necroptosis pathway (Fig. 6a). Interestingly, after administration of RIPA-56 with HFD for 14 days, the increase in body weight and blood glucose level and the deterioration of kidney function indicated by BUN and urine ACR were attenuated compared with the db-HFD group (Fig. 6b). Pathological analysis of mouse kidney tissues showed glomerular hypertrophy, mesangial matrix expansion, tubule dilation, and tubule cell vacuolar degeneration in the db-HFD mice (Fig. 6c). RIPA-56 treatment for 36 days significantly improved the above-mentioned pathological changes (Fig. 6c, d). Meanwhile, the levels of the kidney injury indicator NGAL decreased significantly in the db-HFD+R group (Fig. 6e). The necroptosis marker p-MLKL was expressed in the renal tubules of the db-HFD mice; whereas, RIPA-56 treatment reduced the levels of p-MLKL (Fig. 6f). Enhanced necroptosis pathway activity represented by increased levels of p-RIPK1, p-RIPK3, and p-MLKL was markedly decreased by RIPA-56 treatment in db-HFD+R mice (Fig. 6g, h). These findings suggested that RIPA-56 treatment could prevent HFD-induced necroptosis of RTECs and alleviated renal damage.

RIPA-56 Reduced Necroinflammation and Lipid Accumulation in Renal Tissue of HFD-Fed db/db Mice

To clarify the protective effects of RIPA-56 against nephropathy in db-HFD mice, RNA from wt-HFD and db-HFD mouse kidneys treated with or without RIPA-56 for 36 days was extracted and subjected to RNA-sequencing to identify differentially expressed genes and markedly changed pathways. Signal pathway enrichment analysis was performed on the differentially expressed genes of the db-HFD versus wt-HFD groups using the KEGG database. A total of 39 pathways were upregulated in the kidneys from db-HFD mice compared with kidneys from wt-HFD mice, including metabolic pathways and inflammation-related signaling pathways (Fig. 7a). Compared with the gene expression profile of the kidneys of the db-HFD group, a total of 55 pathways were downregulated in the db-HFD+R group. The diabetes-related entries such as "Type I diabetes mellitus" and "Type II diabetes mellitus," and metabolic pathways were greatly suppressed. More importantly, major inflammatory pathways including the TNF, IL17, NF-κB, and Toll-like receptor signaling pathways were

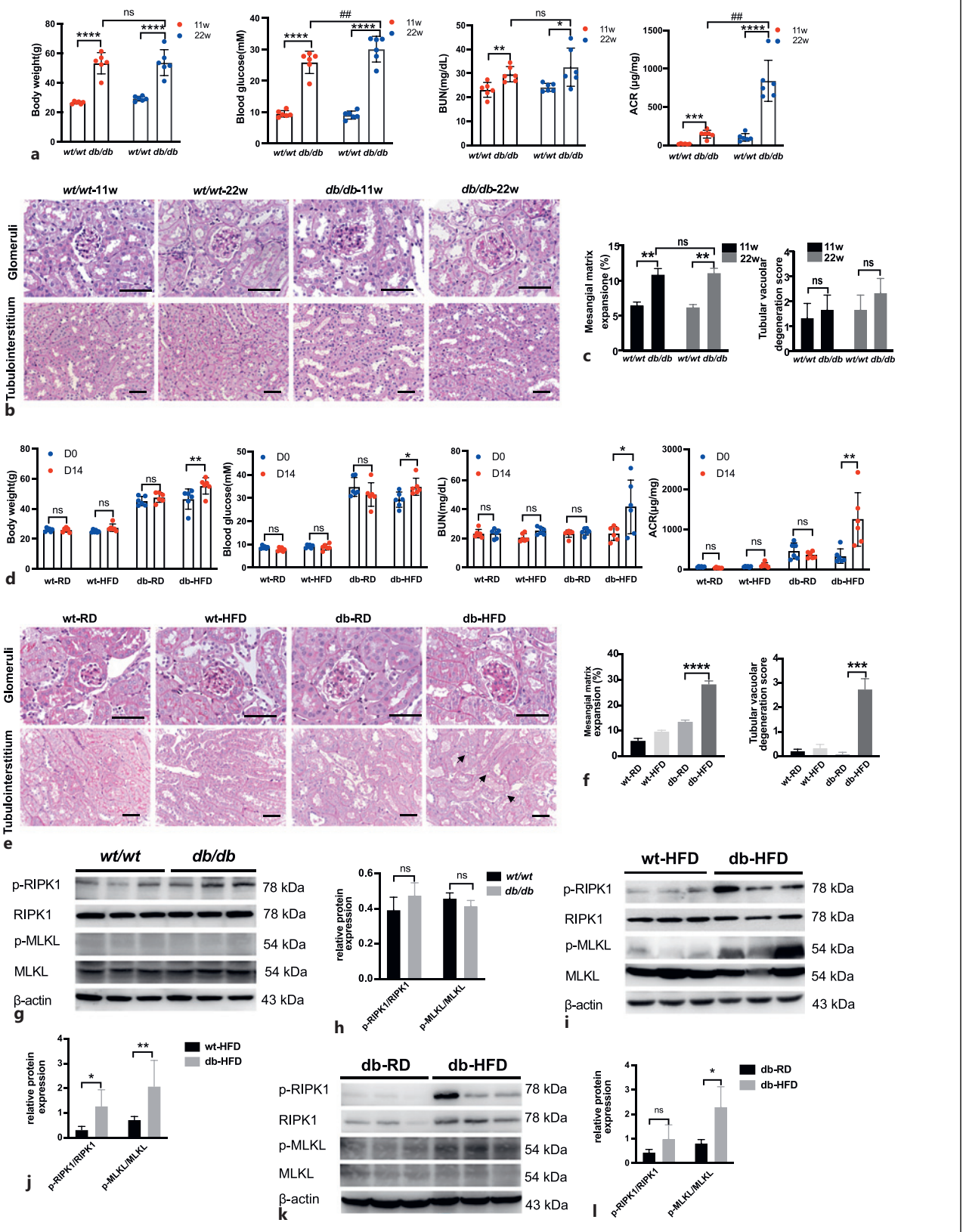

(For legend see next page.)

downregulated. "Necroptosis" was also enriched in the downregulated pathways (Fig. 7b). Changes in the expression of the inflammatory genes such as *Tnf*, *Il1b*, *Ccl2*, and *Cxcl2* were confirmed by quantitative real-time reverse transcription PCR (Fig. 7c). Consequently, macrophage infiltration in the tubulointerstitium was decreased after RIPA-56 treatment (Fig. 7d). Expression level of genes that promote lipid metabolism (*Ppara*, *Ppargc1a, Acox1*, *Cpt1a*, *Cd36*, and *Rxra*) were suppressed in db-HFD mice but were upregulated after RIPA-56 treatment (Fig. 7f). Lipid metabolism was also observed using oil red O staining and electron microscopy. There was very strong oil red O staining in the tubules of db-HFD mice but almost no staining in RIPA-56 treated mice (Fig. 7g). Electron microscopy revealed typical lipid droplets as ring-shaped dots in the tubules of db-HFD mice; whereas RIPA-56 treatment greatly decreased the number of lipid droplets in the tubules of db-HFD mice (Fig. 7g). These data indicated that RIPA-56 might alleviate renal damage in DKD by inhibiting necroinflammation and reducing lipid accumulation.

Discussion

The incidence of DKD has increased significantly with the worldwide epidemic of diabetes. Renal parenchymal cell death was observed during the progression of DKD [3, 22, 23]. Necroptosis is a form of pro-inflammatory cell death regulated by phosphorylation of the kinase RIPK1/RIPK3/MLKL cascade [4]. In recent years, researchers have begun to focus on the possible role of necroptosis in DKD. For example, Xu et al. [24] observed elevated expression of RIPK1, RIPK3, and MLKL in renal biopsies from patients with DKD, mainly localized in podocytes. Meanwhile, Imamura et al. found positive RIPK3 staining in the tubulointerstitial region in allograft biopsies of patients with diabetic nephropathy and tubulointerstitial fibrosis [25]. Recently, Wang et al. found positive staining of p-MLKL in glomerular cells and some tubular cells in kidney tissues from patients with DKD [26]. These studies suggested that DKD involves necroptosis of glomerular and tubular cells. However, the limited number of study cases and the fact that previous studies on necroptosis mainly focused on podocytes both indicate that the role of tubular epithelial cell necroptosis in the occurrence and progression of renal injury in DKD requires further investigation.

In the present study, the role of necroptosis in DKD was clarified initially by staining for the necroptosis pathway executor p-MLKL in renal biopsies, which showed that p-MLKL was most significantly expressed in RTECs, but barely in the glomeruli. p-MLKL levels in the tubulointerstitium correlated positively with the degree of renal function reduction, systemic inflammation, and the degree of pathological damage to the glomeruli and tubules of patients with DKD. Next, stimulation of HK-2 cells with high glucose, PA, albumin, and glycosylation end products to mimic DKD-related pathogenic factors showed that only high glucose combined with fatty acid (PA) increased p-MLKL levels and its cell membrane translocation, indicating necroptosis pathway activation. Oil red O and p-MLKL staining in the kidney tissues of patients with DKD showed that lipid deposition correlated positively with the p-MLKL levels in the tubules. These results suggested that necroptosis of renal tubular cells exists in human DKD and is involved in the progression of renal injury. Synergistic stimulation by fatty acids and high glucose might induce necroptosis in RTECs in DKD.

Fig. 5. Nephropathy was developed in *db/db* mice fed an RD and was aggravated in *db/db* mice fed an HFD. **a** Body weight, fasting blood glucose, BUN and ACR were compared in *wt/wt* and *db/db* mice of 11 weeks old and 22 weeks old ($n = 6$). $^{*}p < 0.05$, $^{**}p < 0.01$, $^{****}p < 0.0001$ compared to *wt/wt* mice; $^{\#\#}p < 0.01$ compared to *db/db* mice at 11 weeks old. **b** PAS staining of different groups of mice. Glomeruli and tubulointerstitium are displayed separately. Scale bar, 50 μm. **c** Statistic analysis of mesangial matrix expansion and tubular vacuolar degeneration score in different groups of mice ($n = 3$). $^{**}p < 0.01$ compared to *wt/wt* mice. **d** Body weight, fasting blood glucose, BUN and ACR were compared in different groups of mice ($n = 6$). $^{*}p < 0.05$, $^{**}p < 0.01$ compared to db-HFD mice (D0). **e** PAS staining of different groups of mice. Glomeruli and tubulointerstitium are displayed separately. Black arrows indicate tubular vacuolar degeneration. Scale bar, 50 μm. **f** Statistic analysis of mesangial matrix expansion and tubular vacuolar degeneration score in different groups of mice. $^{***}p < 0.001$, $^{****}p < 0.0001$ compared to db-RD group. **g**–**h** Representative Western blots and statistical analysis of expression levels of p-RIPK1/RIPK1, p-MLKL/MLKL in *wt/wt* and *db/db* mouse kidneys. $n = 3$. ns: not significant. **i**–**j** Representative Western blots and statistical analysis of expression levels of p-RIPK1/RIPK1, p-MLKL/MLKL in wt-HFD and db-HFD mouse kidneys. $n = 3$. $^{*}p < 0.05$, $^{**}p < 0.01$ compared to wt-HFD. **k**–**l** Representative Western blots and statistical analysis of expression levels of p-RIPK1/RIPK1, p-MLKL/MLKL in db-RD and db-HFD mouse kidneys. $n = 3$. $^{*}p < 0.05$ compared to db-RD.

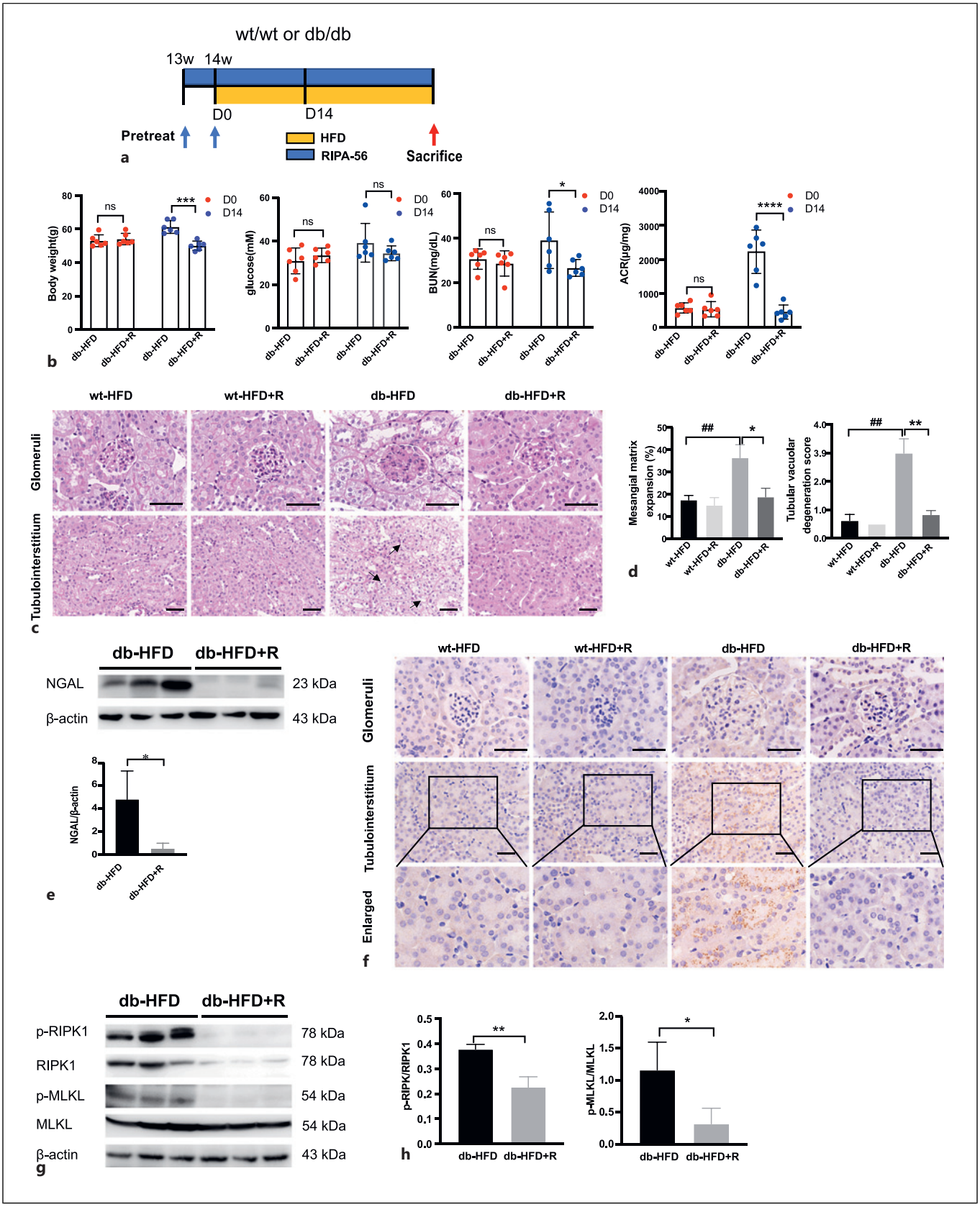

6

(For legend see next page.)

The classical diabetic mouse model (*db/db* mice) has minimal renal pathological damages despite the presence of proteinuria. Therefore, previous studies have used different interventions, such as unilateral nephrectomy [27] or knockout of specific genes (e.g., *eNOS*) [28] in *db/db* mice, as well as feeding them high protein [29] or high-fat diets [30] to accelerate the progression of DKD. To validate the observations in patients with DKD and on HK-2 cells, an HFD protocol was developed for the *db/db* mouse model. The *db/db* mice fed with RD showed early clinical manifestations of DKD with only mild mesangial matrix expansion, no significant pathological changes in the renal tubulointerstitium, and no activation of necroptosis pathways. The renal injury in the HFD-fed *db/db* mice was aggravated by the increase of BUN and ACR levels, the further expansion of the mesangial matrix, and the increase of tubular injury. In addition, the levels of p-RIPK1, p-RIPK3, and p-MLKL increased significantly in the renal tissues of the db-HFD mice. The histochemical staining of p-MLKL showed that RTECs were the main activation site of necroptosis. The accelerating effect of lipid damage on DKD was also observed by Kotake et al. [31] in a unilateral nephrectomized DKD model of Torii obese rats. In that model, ectopic accumulation of lysolecithin in the tubulointerstitial region and significant upregulation of perilipin, a major component of lipid droplets in RTECs, were observed. Lipotoxicity in RTECs increased the production of mitochondrial reactive oxygen species, accelerating cell death, which suggested that lipid metabolism perturbation might be one mechanism that promotes the rapid decline in renal function in patients with DKD [32].

Several inhibitors have been developed for RIPK1, the key kinase of the necroptosis pathway, including Nec-1, necrostatin-1s, compound-71, and RIPA-56 [33–36], and some of them are in phase I and phase II clinical trails. RIPA-56 is a highly selective and metabolically stable RIPK1 inhibitor with an IC50 of 13 nM, which was initially developed for anti-aging and sperm degeneration studies [37, 38]. Subsequently, RIPA-56 was proven to improve steatosis, inflammation and fibrosis in nonalcoholic steatohepatitis in HFD-fed mice [18]. In the present study, 5 weeks of chronic oral administration of RIPA-56 to db-HFD mice suppressed the increased body weight, blood glucose level, and decreased renal function caused by the HFD. After 36 days of oral treatment, the pathological damage to renal tissues was alleviated, and both glomerular lesions and tubulointerstitial damage were relieved. RIPA-56 treatment also significantly inhibited the activation of RIPK1 kinase and decreased the levels of downstream p-MLKL in mouse kidney tissues, effectively inhibiting the necroptosis pathway. Consequently, RIPA-56 treatment significantly decreased the inflammatory gene expression and macrophage infiltration. Transcriptome analysis showed significant upregulation of genes related to fatty acid metabolism after RIPA-56 treatment, and the lipid accumulation in the kidney tissue was significantly decreased. Therefore, the results of current study provide evidence that RIPK1 inhibition and subsequent downstream necrosome inactivation improve the histological features of DKD, relieve inflammation, and maintain lipid homeostasis, supporting the hypothesis that RIPK1 inhibitors may serve as potential therapeutic agents to treat DKD.

The current study still has some limitations. First, although necroptosis of tubular cells correlated with the severity of kidney injury in patients with DKD, the retrospective nature of their recruitment meant that we could not analyze the relationship between necroptosis and renal prognosis in these patients. Future

Fig. 6. RIPA-56 alleviated nephropathy in *db/db* mice fed an HFD. **a** Flow chart of RIPA-56 treatment in *db/db* HFD animal model. RIPA-56 was used to pre-treat the *wt/wt* and *db/db* RD mice at 13 weeks old for 7 days. Then mice were fed an HFD mixed with RIPA-56 for 36 consecutive days. **b** Body weight, fasting blood glucose, BUN and ACR were compared in db-HFD mice treated with or without RIPA-56 at day 0 and after 14 days ($n = 6$). $^{*}p < 0.05$, $^{***}p < 0.001$, and $^{****}p < 0.0001$ compared to db-HFD group (D14). **c** PAS staining of different groups of mice. Glomeruli and tubulointerstitium are displayed separately. Black arrows indicate tubular vacuolar degeneration. Scale bar, 50 μm. **d** Statistic analysis of mesangial matrix expansion and tubular vacuolar degeneration score in different groups of mice. $^{*}p < 0.05$, $^{**}p < 0.01$ compared to db-HFD group; $^{\#\#}p < 0.01$ compared to wt-HFD group. **e** Representative Western blots showing protein expression of NGAL in db-HFD and db-HFD+R mouse kidneys. $^{*}p < 0.05$ compared to db-HFD. **f** Immunohistochemistry staining of p-MLKL in mouse kidney specimens from indicated groups. Scale bar, 50 μm. **g** Representative Western blots showing protein expression of p-RIPK1/RIPK1, p-MLKL/MLKL in db-HFD and db-HFD+R mouse kidneys. **h** The relative protein levels of p-RIPK1/RIPK1, p-MLKL/MLKL to β-actin in different groups ($n = 3$). $^{*}p < 0.05$ $^{**}p < 0.01$ compared to db-HFD.

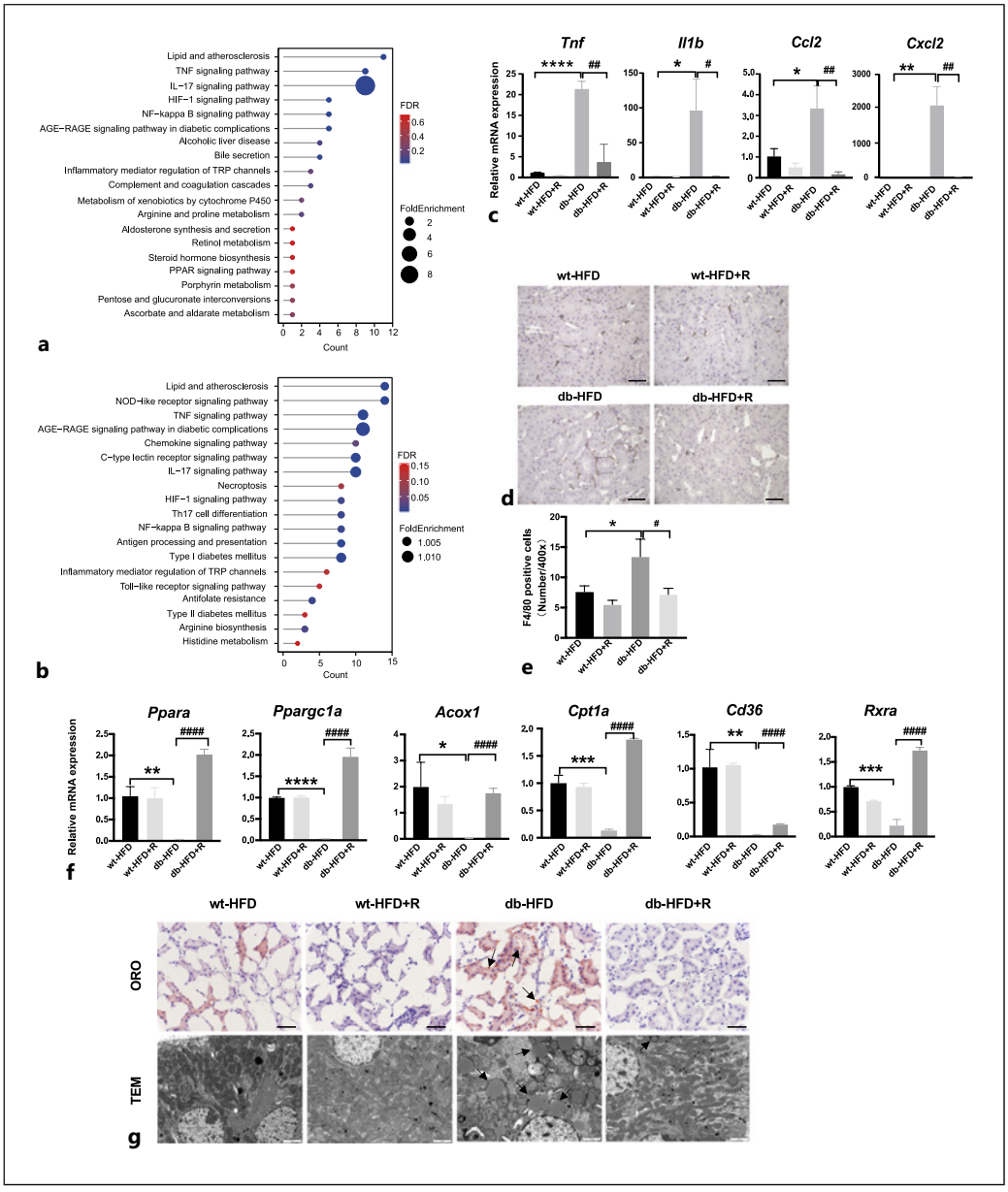

Fig. 7. Changes of necroinflammation and lipid accumulation in db-HFD mice treated with RIPA-56 for 36 days. **a** The representative KEGG pathways of the upregulated DEGs in db-HFD versus wt-HFD groups. **b** The representative KEGG pathways of the downregulated DEGs in db-HFD+R versus db-HFD groups. **c** The mRNA expression of inflammatory mediators in the kidneys of the indicated groups ($n = 3$). $^{*}p < 0.05$, $^{**}p < 0.01$, $^{****}p < 0.0001$ compared to wt-HFD group; $^{\#}p < 0.05$, $^{\#\#}p < 0.01$ compared to db-HFD. **d** Immunohistochemical staining of F4/80 in mouse kidney specimens from indicated groups. Scale bar, 50 μm. **e** Statistic analysis of F4/80 positive cells per ×400 field ($n = 3$). $^{*}p < 0.05$ compared to wt-HFD group; $^{\#}p < 0.05$ compared to db-HFD group. **f** The mRNA expression of lipid metabolism related-genes in the kidneys of indicated groups ($n = 3$). $^{*}p < 0.05$, $^{**}p < 0.01$, $^{***}p < 0.001$, $^{****}p < 0.0001$ compared to wt-HFD group; $^{\#\#\#\#}p < 0.0001$ compared to db-HFD group. **g** Oil red O (scale bar, 50 μm) and electron microscope (scale bar, 2 μm) images from the four indicated groups. Black arrows indicate lipid droplet accumulation. ORO: oil red O; TEM: transmission electron microscope.

prospective cohort studies with large sample sizes are needed. The differences in tissue sample preparation for oil-red O staining (frozen tissue) and p-MLKL staining (paraffin tissue) meant that we could not co-localize the two indicators in DKD samples. In subsequent work, the co-localization of other lipid droplet markers, such as perilipin, with p-MLKL will be performed to further clarify the correlation between disordered lipid metabolism and necroptosis in RTECs. In addition, cellular assays and mouse experiments showed that the combination of high glucose and fatty acid stimulation led to necroptosis in RTECs. However, the specific intracellular signaling pathway remains unknown and requires further investigation. Nevertheless, our findings revealed the role of necroptosis in DKD progression, providing a new therapeutic target for the treatment of DKD.

Acknowledgments

The authors thank Dr. Weiliang Fan and Mr. Tao Xu from Sironax (Beijing, China) for providing the RIPK1 inhibitor RIPA-56.

Statement of Ethics

All animal experiments were reviewed and approved by the Institutional Animal Care and Use Committee (IACUC) of Peking University First Hospital, approval number: J202169. The study using human participants was approved by the Ethics Committee of Peking University First Hospital (approval number: 2022-487), and all patients signed informed consent forms.

Conflict of Interest Statement

The authors have no conflicts of interest to declare.

Funding Sources

This study was supported by grants from the National Natural Science Foundation of China (No. 82130021), the Beijing Young Scientist Program (BJJWZYJH01201910001006), CAMS Innovation Fund for Medical Sciences (2019-I2M-5-046, 2020-JKCS-009), and PKU-Baidu Fund (2020BD026, 2020BD044) to Li Yang and grant from the National Natural Science Foundation of China (No. 82270709) to Ying Chen.

Author Contributions

Qi Yu performed the experiments. Qi Yu and Ying Chen collected, analyzed, and interpreted the data. Ying Chen drafted the manuscript. Youlu Zhao, Shuo Huang, and Wenyan Wu helped collect and assembly the data. Xiaohong Xin analyzed the data of RNA sequencing. Lei Qu conducted the tissue embedding, sectioning, and histological staining. Lei Jiang and Hui Wang performed the semi-quantitation of renal injury. Chengang Xiang, Suxia Wang, and Gang Liu revised the manuscript. Li Yang conceived and supervised the study, interpreted the data, and revised the manuscript.

Data Availability Statement

Data of RNA sequencing for all samples were deposited in Sequence Read Archive (SRA) under accession code PRJNA776423 (http://www.ncbi.nlm.nih.gov/bioproject/776423). All data generated or analyzed during this study are included in this article. Further inquiries can be directed to the corresponding author.

References

1 Tuttle KR, Wong L, St Peter W, Roberts G, Rangaswami J, Mottl A, et al. Moving from evidence to implementation of breakthrough therapies for diabetic kidney disease. Clin J Am Soc Nephrol. 2022;17(7):1092–103.
2 Thomas MC, Cooper ME, Zimmet P. Changing epidemiology of type 2 diabetes mellitus and associated chronic kidney disease. Nat Rev Nephrol. 2016;12(2):73–81.
3 Shen S, Ji C, Wei K. Cellular senescence and regulated cell death of tubular epithelial cells in diabetic kidney disease. Front Endocrinol. 2022;13:924299.
4 Khoury MK, Gupta K, Franco SR, Liu B. Necroptosis in the pathophysiology of disease. Am J Pathol. 2020;190(2):272–85.
5 Bertheloot D, Latz E, Franklin BS. Necroptosis, pyroptosis and apoptosis: an intricate game of cell death. Cell Mol Immunol. 2021;18(5):1106–21.
6 Pasparakis M, Vandenabeele P. Necroptosis and its role in inflammation. Nature. 2015;517(7534):311–20.
7 Weinlich R, Oberst A, Beere HM, Green DR. Necroptosis in development, inflammation and disease. Nat Rev Mol Cell Biol. 2017;18(2):127–36.
8 Tonnus W, Belavgeni A, Beuschlein F, Eisenhofer G, Fassnacht M, Kroiss M, et al. The role of regulated necrosis in endocrine diseases. Nat Rev Endocrinol. 2021;17(8):497–510.
9 Chen A, Feng Y, Lai H, Ju W, Li Z, Li Y, et al. Soluble RARRES1 induces podocyte apoptosis to promote glomerular disease progression. J Clin Invest. 2020;130(10):5523–35.
10 Chen Q, Su Y, Ju Y, Ma K, Li W, Li W. Astragalosides IV protected the renal tubular epithelial cells from free fatty acids-induced injury by reducing oxidative stress and apoptosis. Biomed Pharmacother. 2018;108:679–86.
11 Guo Y, Xie X, Zhao Y, Zhou M, Yang Y, Zhang X. Calcitriol attenuates renal tubular epithelial cells apoptosis via inhibiting p38MAPK signaling in diabetic nephropathy. Acta Diabetol. 2020;57(11):1327–35.
12 Caccamo A, Branca C, Piras IS, Ferreira E, Huentelman MJ, Liang WS, et al. Necroptosis activation in Alzheimer's disease. Nat Neurosci. 2017;20(9):1236–46.
13 Yuan J, Amin P, Ofengeim D. Necroptosis and RIPK1-mediated neuroinflammation in CNS diseases. Nat Rev Neurosci. 2019;20(1):19–33.
14 Rojas J, Bermudez V, Palmar J, Martinez MS, Olivar LC, Nava M, et al. Pancreatic beta cell death: novel potential mechanisms in diabetes therapy. J Diabetes Res. 2018;2018:9601801.
15 Chen Y, Hua Y, Li X, Arslan IM, Zhang W, Meng G. Distinct types of cell death and the implication in diabetic cardiomyopathy. Front Pharmacol. 2020;11:42.
16 Alicic RZ, Rooney MT, Tuttle KR. Diabetic kidney disease: challenges, progress, and possibilities. Clin J Am Soc Nephrol. 2017;12(12):2032–45.
17 Wu WY, Zhou XJ, Sun PP, Yu XJ, Wang SX, Qu L, et al. Interstitial eosinophilic infiltration in diabetic nephropathy is indicative of poor prognosis, with no therapy benefit from steroid. J Diabetes. 2020;12(12):881–94.
18 Majdi A, Aoudjehane L, Ratziu V, Islam T, Afonso MB, Conti F, et al. Inhibition of receptor-interacting protein kinase 1 improves experimental non-alcoholic fatty liver disease. J Hepatol. 2020;72(4):627–35.
19 Chi D, Chen Y, Xiang C, Yao W, Wang H, Zheng X, et al. Human amnion epithelial cells and their derived exosomes alleviate sepsis-associated acute kidney injury via mitigating endothelial dysfunction. Front Med. 2022;9:829606.
20 Kang X, Chen Y, Xin X, Liu M, Ma Y, Ren Y, et al. Human amniotic epithelial cells and their derived exosomes protect against cisplatin-induced acute kidney injury without compromising its antitumor activity in mice. Front Cell Dev Biol. 2021;9:752053.
21 Tervaert TWC, Mooyaart AL, Amann K, Cohen AH, Cook HT, Drachenberg CB, et al. Pathologic classification of diabetic nephropathy. J Am Soc Nephrol. 2010;21(4):556–63.
22 Bălăşescu E, Ion DA, Cioplea M, Zurac S. Caspases, cell death and diabetic nephropathy. Rom J Intern Med. 2015;53(4):296–303.

23 Erekat NS. Programmed cell death in diabetic nephropathy: a review of apoptosis, autophagy, and necroptosis. Med Sci Monit. 2022;28:e937766.
24 Xu Y, Gao H, Hu Y, Fang Y, Qi C, Huang J, et al. High glucose-induced apoptosis and necroptosis in podocytes is regulated by UCHL1 via RIPK1/RIPK3 pathway. Exp Cell Res. 2019;382(2):111463.
25 Imamura M, Moon JS, Chung KP, Nakahira K, Muthukumar T, Shingarev R, et al. RIPK3 promotes kidney fibrosis via AKT-dependent ATP citrate lyase. JCI Insight. 2018;3(3):e94979.
26 Wang X, Liu XQ, Jiang L, Huang YB, Zeng HX, Zhu QJ, et al. Paeoniflorin directly binds to TNFR1 to regulate podocyte necroptosis in diabetic kidney disease. Front Pharmacol. 2022;13:966645.
27 Fan Y, Zhang J, Xiao W, Lee K, Li Z, Wen J, et al. Rtn1a-Mediated endoplasmic reticulum stress in podocyte injury and diabetic nephropathy. Sci Rep. 2017;7(1):323.
28 Zhao HJ, Wang S, Cheng H, Zhang MZ, Takahashi T, Fogo AB, et al. Endothelial nitric oxide synthase deficiency produces accelerated nephropathy in diabetic mice. J Am Soc Nephrol. 2006;17(10):2664–9.
29 Norgaard SA, Briand F, Sand FW, Galsgaard ED, Sondergaard H, Sorensen DB, et al. Nephropathy in diabetic db/db mice is accelerated by high protein diet and improved by the SGLT2 inhibitor dapagliflozin. Eur J Pharmacol. 2019;860:172537.
30 Zhang HM, Dang H, Kamat A, Yeh CK, Zhang BX. Geldanamycin derivative ameliorates high fat diet-induced renal failure in diabetes. PLoS One. 2012;7(3):e32746.
31 Kotake H, Yamada S, Ogura Y, Watanabe S, Inoue K, Ichikawa D, et al. Endurance exercise training-attenuated diabetic kidney disease with muscle weakness in spontaneously diabetic Torii fatty rats. Kidney Blood Press Res. 2022;47(3):203–18.
32 Opazo-Rios L, Mas S, Marin-Royo G, Mezzano S, Gomez-Guerrero C, Moreno JA, et al. Lipotoxicity and diabetic nephropathy: novel mechanistic insights and therapeutic opportunities. Int J Mol Sci. 2020;21(7):2632.
33 Cao L, Mu W. Necrostatin-1 and necroptosis inhibition: pathophysiology and therapeutic implications. Pharmacol Res. 2021;163:105297.
34 Wang Q, Zhou T, Liu Z, Ren J, Phan N, Gupta K, et al. Inhibition of receptor-interacting protein kinase 1 with Necrostatin-1s ameliorates disease progression in elastase-induced mouse abdominal aortic aneurysm model. Sci Rep. 2017;7:42159.
35 Wang JN, Liu MM, Wang F, Wei B, Yang Q, Cai YT, et al. RIPK1 inhibitor Cpd-71 attenuates renal dysfunction in cisplatin-treated mice via attenuating necroptosis, inflammation and oxidative stress. Clin Sci. 2019;133(14):1609–27.
36 Ren Y, Su Y, Sun L, He S, Meng L, Liao D, et al. Discovery of a highly potent, selective, and metabolically stable inhibitor of receptor-interacting protein 1 (RIP1) for the treatment of systemic inflammatory response syndrome. J Med Chem. 2017;60(3):972–86.
37 Li D, Meng L, Xu T, Su Y, Liu X, Zhang Z, et al. RIPK1-RIPK3-MLKL-dependent necrosis promotes the aging of mouse male reproductive system. Elife. 2017;6:e27692.
38 Xie Y, Chen H, Luo D, Yang X, Yao J, Zhang C, et al. Inhibiting necroptosis of spermatogonial stem cell as a novel strategy for male fertility preservation. Stem Cell Dev. 2020;29(8):475–87.